NeuroImage 61 (2012) 195–205

Contents lists available at SciVerse ScienceDirect

NeuroImage

journal homepage: www.elsevier.com/locate/ynimg

A multi-modal investigation of behavioral adjustment: Post-error slowing is associated with white matter characteristics

Anders M. Fjell [a,b,*], Lars T. Westlye [a], Inge K. Amlien [a], Kristine B. Walhovd [a,b]

[a] Center for the Study of Human Cognition, Department of Psychology, University of Oslo, Pb 1084, 0317 Oslo, Norway
[b] Department of Physical Medicine and Rehabilitation, Unit of Neuropsychology, Oslo University Hospital, Norway

ARTICLE INFO

Article history:
Accepted 3 March 2012
Available online 12 March 2012

Keywords:
Cognitive control
Post-error slowing
Diffusion tensor imaging
Magnetic resonance imaging
Morphometry
Aging

ABSTRACT

When people make mistakes in speeded cognitive tasks, their response time on the next trial will typically be slower. This is referred to as post-error slowing (PES), and is important for optimization of performance, but its exact function remains to be decided. However, although PES is relatively stable over time, we have almost no knowledge about how PES is affected by structural brain characteristics. The aim of this study was to test to what extent white matter (WM) macro- and microstructure can account for individual differences in PES. PES was calculated for 255 healthy participants who performed a modified version of the Eriksen flanker task and underwent structural magnetic resonance imaging and diffusion tensor imaging (DTI). PES was positively related to WM volume in the caudal and rostral middle and superior frontal, medial orbitofrontal gyri and pars orbitalis. DTI analyses with tract-based spatial statistics (TBSS) showed that mean diffusivity in the superior longitudinal fasciculus, inferior fronto-occipital fasciculus and anterior thalamic radiation, as well as axial diffusivity in the corpus callosum, was negatively related to PES. Path analysis demonstrated that WM micro- and macrostructure were complementary in accounting for PES. It is concluded that individual differences in WM characteristics can partly explain why some people are better at adjusting their behavior in response to poor performance than others.

© 2012 Elsevier Inc. All rights reserved.

Introduction

After commission of an error, the performance monitoring system will induce a general adjustment to impose more controlled cognition, resulting in a slower response on the next trial. This phenomenon is referred to as post-error slowing (PES) (Rabbitt, 1966). The exact function of PES is not yet known, but it likely crucial for optimization of performance (Danielmeier and Ullsperger, 2011). Medial frontal cortex (MFC) is especially important for error monitoring and adjustments of attention (Ridderinkhof et al., 2004), and it was recently shown that upon the occurrence of errors, posterior MFC selectively drove attention toward task-relevant information, resulting in motor adaptation observed as PES (Danielmeier et al., 2011). However, even though there are huge individual differences in the degree to which persons adjust their response thresholds after commission of an error, we have almost no knowledge about how normal variations in structural brain characteristics are related to PES. One hypothesis would be that PES is modulated by the integrity of the brain's white matter (WM). To allow efficient monitoring of performance in speeded cognitive tasks, rapid interactions and cross-talk between different prefrontal areas, and between prefrontal areas and other brain regions, are necessary. These interactions place great demands on the long-distance projection fibers. Thus, the aim of the present study was to test how individual differences in PES are related to WM macro- and microstructure in an adult lifespan sample. The stability of PES over time (Danielmeier and Ullsperger, 2011) further underscores the importance of understanding structural underpinnings of the phenomenon.

The rationale for hypothesizing a relationship between WM integrity and performance monitoring and adjustment is based on several sources of evidence. An important line of studies has measured the error-related negativity (ERN), an electrophysiological response that can be seen within 100 ms after the commission of an error (Bernstein et al., 1995; Falkenstein et al., 1991; Gehring et al., 1993). ERN assumedly reflects a combination of error or conflict awareness and behavioral adjustment processes, and is likely generated in the cingulate (Agam et al., 2011; Debener et al., 2005). This makes the cingulum bundle an important information highway between cingulate cortex and other parts of the brain. The integrity of such WM connections can be quantified by diffusion tensor imaging (DTI), which allows for in vivo quantification of the degree and directionality of water diffusion, and is sensitive to microstructural properties of the brain tissue. Fractional anisotropy (FA), derived from DTI, reflects the directionality of water diffusion in the tissue, and is generally regarded as a measure of WM integrity. ERN amplitude has been found to be related to FA of the posterior cingulum bundle

* Corresponding author at: Dept. of Psychology, Pb. 1094 Blindern, 0317 Oslo, Norway. Fax: +47 22 84 50 01.
E-mail address: andersmf@psykologi.uio.no (A.M. Fjell).

1053-8119/$ – see front matter © 2012 Elsevier Inc. All rights reserved.
doi:10.1016/j.neuroimage.2012.03.007

(Westlye et al., 2009), and a multi-modal study found that faster error correction was associated with higher FA in the posterior cingulate (Agam et al., 2011).

The above described findings indicate that WM integrity is indeed important for the efficiency of the performance monitoring system. However, there has been a lack of efforts to directly map if and how PES is related to such characteristics of the brain. An exception is a recent important study of 20 young and healthy participants where a correlation was found between PES and fractional anisotropy (FA) in WM beneath posterior MFC regions connected to the motor inhibition system (Danielmeier et al., 2011). Thus, although the exact neuroanatomical and neurophysiological principles are yet to be discovered, there are reasons to expect that the ability to adjust behavior in response to errors is related to WM integrity, in line with several previous lesion studies (Gehring and Knight, 2000; Hogan et al., 2006; Stemmer et al., 2004; Ullsperger and von Cramon, 2006).

Still, no large-scale efforts have been undertaken to systematically investigate how PES relates to different properties of WM, which is the aim of the present study. WM volume was measured in 68 gyral regions using an automated segmentation method (Fjell et al., 2008; Salat et al., 2009), while microstructure was measured by DTI data analyzed with full-brain tract-based spatial statistics (TBSS) (Smith et al., 2006). Based on the notion that the integrity of WM would be related to the participants' ability to efficiently adjust behavior in response to errors, we hypothesized that PES would be positively correlated with WM volume and FA, and negatively with degree of diffusion along (axial diffusion, AD) and across (RD) the main direction of the diffusion tensor, as well as the mean diffusion (MD). Reduced AD has been related to axonal loss in animal models (Song et al., 2003), and increased AD will also result in increased FA if no change in RD is seen. However, several studies have found increased AD in healthy aging and Alzheimer's disease (Agosta et al., 2011; Madden et al., 2012), and so increased AD may be an indication of reduced WM fiber integrity in these conditions. Thus, we expected a negative relationship between PES and AD. Further, resting on the very limited number of studies exploring the neuroanatomical basis of PES in healthy individuals, we expected effects in areas of the frontal cortex, including connecting pathways between the pre-SMA, lateral inferior frontal cortex (IFC) and the subthalamic nuclei (STN) (Aron et al., 2007; Danielmeier and Ullsperger, 2011). Patients with thalamic lesions show deficient error processing, including PES (Peterburs et al., 2011; Seifert et al., 2011). Thus, in addition to WM volume and microstructure, we also included thalamic volume as a final variable of interest.

Materials and methods

Sample

The sample was drawn from the first wave of a longitudinal research project at the Center for the Study of Human Cognition at the University of Oslo: *Cognition and Plasticity through the Life-Span* (Fjell et al., 2008; Westlye et al., 2009). The study was approved by the Regional Ethical Committee of Southern Norway (REK-Sør). The participants were recruited through newspaper ads and among students and employees of the University of Oslo. Further details regarding recruitment and enrolment are given elsewhere (Fjell et al., 2008; Westlye et al., 2009). We obtained written informed consent from all participants. All subjects were right handed native Norwegian speakers. The participants were screened using a standardized health interview on telephone prior to inclusion in the study. History of neurological or psychiatric conditions thought to affect normal cerebral functioning; including clinically significant stroke, serious head injury, untreated hypertension, diabetes and use of psychoactive drugs within the last two years were exclusion criteria. Further, participants reporting worries concerning their cognitive status, including memory function, were excluded. All subjects scored <16 on Beck Depression Inventory (BDI) (Beck and Steer, 1987) and subjects above 40 years of age ≥26 on Mini Mental State Examination (MMSE) (Bravo and Hebert, 1997; Folstein et al., 1975). General cognitive abilities were assessed by Wechsler Abbreviated Scale of Intelligence (WASI) (Wechsler, 1999). All participants scored within normal IQ range. All MR scans were examined by a specialist in neuroradiology and excluded if containing significant anomalies including signs of vascular insults.

270 participants fulfilling the above criteria completed the Eriksen flanker task (see below). Of these, 15 participants were excluded due to <5 correct responses after an error response. Thus, the final n was 255 (147 females/ 108 males), with a mean age of 48.3 (20–83 years), MMSE of 29.1 (participants >40 years), 15.7 years of education (4–26, lacking information for two participants) and full scale IQ of 114.1 (92–141).

Experimental task

We administered a modified version of the Eriksen flanker task (Eriksen and Eriksen, 1974), described in details elsewhere (Westlye et al., 2009), similar to the task used by Debener et al. (Debener et al., 2005). A brief overview of the main features of the task is given in Fig. 1. The stimuli were horizontal arrows of length 1° pointing either to the right or the left displayed in a vertical stack 2.5° high. Subjects were to respond as accurately and quickly as possible by button presses indicating which direction the middle arrow was pointing. Each trial consisted of the following stimuli; first, a fixation cross was presented for a random interval ranging between 1200 and 1800 ms. Then the four flanker arrows were presented for 80 ms before the target arrow was presented for 30 ms along with the flanker arrows. The flanker arrows were presented prior to the target to increase prepotent responding and make the task more difficult. At presentation of the target, the task was to push the left button with the left index finger if the target was pointing to the left, and the right button with the right index finger if the target was pointing to the right. Based on the mean reaction time (RT) for the 20 first consecutive trials, an individually adjusted RT criterion (10% above mean RT of the 20 initial trials) was set. After every subsequent third trial either with RT exceeding this criterion or with response omission, a message occurred on screen for 1 s instructing the participant to respond faster. Before the experiment, a training session of 20 trials was administered in order to familiarize the participant with the task.

On average, 7.7 instructions to respond faster were given during the complete experiment (sd = 13.7). Number of instructions did not correlate with intellectual ability as quantified by full-scale IQ (FSIQ) from WASI ($r = -.00$, $p = .96$), education ($r = -.01$, $p = .92$) or MMSE score ($r = -.01$, $p = .86$), or with age when median RT was partialled out ($r = .00$, $p = .98$). Instructions to respond faster correlated −.24 with number of correct responses in the congruent condition ($p < .001$), while no significant correlation was found in the incongruent condition ($r = -.06$, n.s.). The rationale for using this procedure was to increase the demand to respond swiftly and

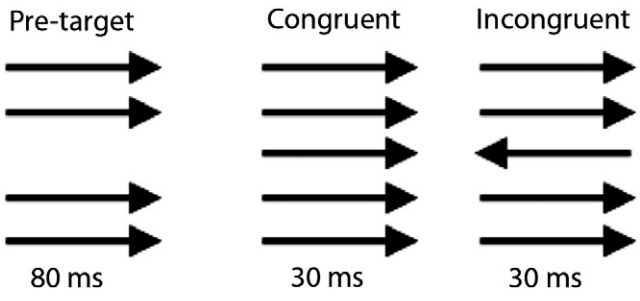

Fig. 1. Flanker task. For details, please consult the main text.

thus increase task difficulty, to increase the participants' motivation for rapid responses and to enhance their attentional investments in the task. We expected that this would reduce variability due to random attentional drifts etc., and leave us with a response measure more closely related to task-focused central nervous system function.

Responses were obtained on a PST Serial Response Box, and the experimental procedures and responses were collected using E-prime (Psychological Software Tools, Pittsburgh, PA) software. There were two experimental task conditions; congruent and incongruent. In the congruent condition all arrows were pointing in the same direction. In the incongruent condition, the middle arrow was pointing towards the opposite side as the flanker arrows. The task included 416 trials with a short break half way. The probability of an incongruent trial was 50% in a randomized fashion. The correlation between mean RT across subjects per trial and trial number was $r = .04$ ($p = .51$), indicating that no clear linear drift in RT existed throughout the course of the task session. This was probably partly due to the training session administered before the experiment, and the feedback presented on screen in response to slow RTs or response omissions (see above).

For statistical analyses, we excluded the first 10 trials, as well as the 10 trials with the fastest and the slowest RTs, for each condition separately. This was done because it is difficult to decide whether extreme responses represent variations of the real cognitive processes under study, or whether they result from random noise due to factors such as the participant missing the button, having a single lapse of attention during the course of a long speeded task, etc. Thus a simple way of reducing the possibility that such noise contaminate the data, without biasing the results in either direction, is to exclude the extreme ends of the RT distribution for all participants.

Since RTs to incongruent stimuli tend to be slower than for congruent stimuli, and more errors are committed in the incongruent condition (Eriksen and Eriksen, 1974), analyzing PES averaged across stimulus categories would likely reduce the observed PES. Accordingly, PES was analysed for each stimulus category separately. Mean RT for each correct congruent trial following an error trial was calculated, as well as mean RT for each correct congruent trial following a correct trial. PES was calculated as the difference between these, divided by the mean RT across all correct congruent trials. In addition, post-hoc analyses were computed with non-normalized PES values (i.e. not divided by mean RT). For incongruent trials, the difference between post-error and post-correct trials was not significant (see below). This could be caused by increased selective attention after errors, which may enhance PES for congruent while counteract PES for incongruent stimuli. Danielmeier and Ullsperger (2011) argue that PES is associated with both inhibition in the motor system and adjustments in task-related brain areas. The latter may be related to attentional processes or post-error focusing, and slowing and post-error focusing could therefore counteract each other (Verguts et al., 2011). Due to the lack of a significant PES in the incongruent condition in the present study, further analyses were confined to congruent trials only.

MR acquisition

Imaging data were collected using a 12 channel head coil on a 1.5T Siemens Avanto scanner (Siemens Medical Solutions, Erlangen, Germany) at Oslo University Hospital, Rikshospitalet. For diffusion weighted imaging a single-shot twice-refocused spin echo echo planar imaging (EPI) pulse sequence with 30 diffusion sensitized gradient directions and the following parameters was used: repetition time (TR)/echo time (TE) = 8200 ms/82 ms, b-value = 700 s/mm^2, voxel size = 2.0 × 2.0 × 2.0 mm. This sequence is optimized to minimize eddy current-induced image distortions (Reese et al., 2003). The sequence was repeated in two successive runs with 10 b = 0 in addition to 30 diffusion weighted images collected per acquisition. The two acquisitions were combined during post-processing to increase signal-to-noise-ratio (SNR). Each volume consisted of 64 axial slices. Total scanning time was 11 min, 21 s.

The pulse sequence used for volumetric analyses were two repeated T1-weighted Magnetization Prepared Rapid Gradient Echo (MP-RAGE), with the following parameters: TR/TE/TI/FA = 2400 ms/3.61 ms/1000 ms/8°, matrix 192 × 192, field of view = 240. Scanning time was 7 min, 42 s. Each volume consisted of 160 sagittal slices with voxel size 1.25 × 1.25 × 1.20 mm. The two MP-RAGEs were averaged during post-processing to increase SNR. All datasets were processed and analysed at the Neuroimaging Analysis Lab, Center for the Study of Human Cognition, University of Oslo, with additional use of computing resources from the Titan High Performance Computing facilities (http://hpc.uio.no/index.php/Titan) at the University of Oslo.

DTI analysis

Image analyses and tensor calculations were done using FSL (Smith et al., 2004; Woolrich et al., 2009) (http://www.fmrib.ox.ac.uk/fsl/index.html). Initially, each DTI volume was affine registered to the T2-weighted b = 0 volume using FLIRT (Jenkinson and Smith, 2001). This corrected for motion between scans and residual eddy-current distortions present in the diffusion weighted volumes. In order to preserve the orientational information after motion correction, we reoriented each volume's B matrix by applying the corresponding transformation matrix from the motion-correction procedure. After removal of non-brain tissue (Smith, 2002), least square fits were performed to estimate the FA, eigenvector and eigenvalue maps. We defined radial diffusion (RD) as the mean of the second and third eigenvalue ($(\lambda_2 + \lambda_3)/2$) and mean diffusivity (MD) as the mean of all three eigenvalues. Next, all individuals' FA volumes were skeletonised and transformed into a common space as employed in TBSS (Smith et al., 2006, 2007). Briefly, all volumes were nonlinearly warped to the FMRIB58_FA template, which is supplied with FSL, by use of local deformation procedures performed by FNIRT (Andersson et al., 2007a, 2007b), a non-linear registration toolkit using a b-spline representation of the registration warp field (Rueckert et al., 1999).

All warped FA volumes were visually inspected for accuracy, which is especially pertinent when analyzing life-span datasets with relatively large individual variability in brain size and architecture. We have previously shown that FNIRT performed the native-to-standard warping adequately across age groups (Westlye et al., 2010).

Next, a mean FA volume of all subjects was generated and thinned to create a mean FA skeleton representing the centers of all common tracts. We binarized the mean skeleton at FA > .20 to reduce the likelihood of partial voluming in the borders between tissue classes, yielding a mask of 128267 WM voxels. Individual FA values were warped onto this mean skeleton mask by searching perpendicular from the skeleton for maximum FA values. Using maximum FA values from the centers of the tracts further minimizes confounding effects due to partial voluming (Smith et al., 2006). The resulting tract invariant skeletons for each participant were fed into voxel-wise permutation based cross-subject statistics. Similar warping and analyses were employed on AD, RD, and MD data, yielding AD, RD and MD skeletons sampled from voxels with FA > .20. The total volume of white matter T1 hypointensities was quantified and used as covariate in selected analyses (see Statistical analyses). Hypointensities from T1-weighted images correlate with FLAIR measurements, thereby providing a metric of WM lesions (Rovaris et al., 1999).

Finally, in order to enable comparison with previous studies (see below), we performed probabilistic tractography using selected effect sites as seed regions to delineate the major pathways of which the selected regions were constituents. The local diffusion directions were

calculated using Bayesian Estimation of Diffusion Parameters Obtained using Sampling Techniques (bedpostx), which allows for modeling of several anisotropic compartments within each voxel (Behrens et al., 2003, 2007). Here, we modeled up to two compartments per voxel. The probabilistic tractography was performed using probtrackx, which iteratively samples from the distributions of voxel-wise principal diffusion directions, each time computing a streamline through these local samples to generate a probabilistic distribution on the location of the true streamline. Here, the posterior connectivity distribution was generated using 5000 iterations per voxel. The tractography was performed in the native diffusion space of 60 randomly selected datasets, with each distribution thresholded at the 95. percentile, warped to a common space using FLIRT (Jenkinson and Smith, 2001; Jenkinson et al., 2002) and FNIRT (Andersson et al., 2007a, 2007b), concatenated, and averaged across subjects in order to generate a group template of each connectivity distribution. In order to retain the streamlines of lowest uncertainty across subjects only, the group template was thresholded, binarized, and projected onto a high-resolution 3D map in 3D slicer (http://www.slicer.org/) for visualization.

Volumetric analyses

We estimated regional WM volumes using Freesurfer 4.1 (http://surfer.nmr.mgh.harvard.edu/) by means of an automated surface reconstruction scheme described in detail elsewhere (Dale et al., 1999; Fischl and Dale, 2000; Fischl et al., 1999a, 1999b, 2001; Segonne et al., 2004). Briefly, the cortical surface was automatically parcellated based on (1) the probability of each label at each location in a surface-based atlas space, based on a manually parcellated training set; (2) local curvature information; and (3) contextual information, encoding spatial neighbourhood relationships between labels (conditional probability distributions derived from the manual training set) resulting in 33 surface-based regions (Desikan et al., 2006; Fischl et al., 2004b). WM voxels within a distance of 5 mm from the cortical surface was labelled according to the label of the nearest cortical vertex (Fjell et al., 2008; Salat et al., 2009) yielding 33 bilateral WM parcels, each corresponding to a cortical area. The WM voxels not assigned to a surface area were labelled deep WM. All resulting surface labels were manually inspected for accuracy. Areas segmented as hypointense WM areas ("dark spots") based on the MP-RAGES were not included in the WM volumes. We combined parcels into larger subsets of bilateral lobule based regions (frontal, parietal, temporal and occipital lobe) in addition to the cingulate gyrus, corpus callosum, and total WM. Intracranial volume (ICV) was calculated by an atlas-based normalization procedure (Buckner et al., 2004).

Thalamus was automatically segmented based on the FreeSurfer subcortical processing stream, where a neuroanatomical label is assigned to each voxel in an MRI volume based on probabilistic information automatically estimated from a manually labeled training set (Fischl et al., 2002). The training set included both healthy persons in the age range 18–87 years and a group of Alzheimer's disease patients in the age range 60–87 years, and the classification technique employs a registration procedure that is robust to anatomical variability, including the ventricular enlargement typically associated with aging. The technique has previously been shown to be comparable in accuracy to manual labeling (Fischl et al., 2002, 2004a).

Statistics

Relationships between PES (normalized to mean RT) and WM volumes were tested by partial correlations, where age and ICV were controlled for. PES was recursively correlated with WM volume at four different levels of spatial resolution (Total WM volume, lobar WM volume, lobar hemispheric WM volume, regional WM volume averaged across hemispheres). A procedure with some similarities to the conditional inference tree approach was used. An analysis was performed only if the correlation at the previous level of resolution was significant ($p<.05$). Thus, a significant correlation between PES and total WM volume was followed by analyses of the relationships between volume and PES at the level of lobes. Only the variables at the level of lobes where significant correlations with PES were found would be entered into further analyses on the next level, and so forth. In addition, a separate analysis was run for thalamus volume. All analyses were repeated with sex and task performance (the number of correct responses in each condition) as additional covariates, and with non-normalized PES values.

Table 1
Regional white matter volume and post-error slowing Partial correlations between regional white matter volume and post-error slowing, controlling for the effect of age and intracranial volume.

WM area	Partial r	p <
Total WM	**.15**	.05
Lobes		
Frontal WM	**.22**	.001
Parietal WM	.11	n.s.
Temporal WM	.08	n.s.
Occipital WM	.00	n.s.
Cingulum WM	.09	n.s.
Corpus callosum	.00	n.s.
Frontal hemispheres		
Left Frontal WM	**.24**	.001
Right Frontal WM	**.20**	.001
Frontal ROIs		
Caudal middle frontal	**.18**	.01
Rostral middle frontal	**.14**	.05
Medial orbitofrontal	**.16**	.05
Pars orbitalis	**.15**	.05
Superior frontal	**.19**	.01
Frontal pole	.11	n.s.
Lateral orbitofrontal	.11	n.s.
Pars opercularis	.05	n.s.
Pars triangularis	.02	n.s.

Bold indicates $p<.05$.

For DTI, voxel based DTI analyses were performed using permutation based statistics (Nichols and Holmes, 2002) as implemented in randomise, part of FSL. GLMs were run across the skeleton with age as covariates for PES. Threshold Free Cluster Enhancement (TFCE) (Smith and Nichols, 2009) was used for statistical inference. 5000 permutations were performed for each contrast. Statistical p-value maps were thresholded at $p<.05$ corrected for multiple comparisons across space and displayed as color coded overlays. Next, mean values from each voxel with $p<.05$ from each analysis (RD, MD, AD, FA) were extracted for each participant, and fed into partial correlation analyses (controlled for age) with PES. This was done to enable estimation of effect sizes in terms of correlation coefficients. As these analyses were restricted to voxels where significant relationships with PES already had been established, these must not be regarded as part of the hypothesis testing. Similar to the morphometry analyses, the partial correlation analyses were repeated with sex, task performance and total volume of WM hypointensities from the T1-weighted scans as additional covariates, and with non-normalized PES values.

All significant analyses were repeated with statistical outliers excluded, defined as participants for whom studentized deleted residuals >3 or <-3. This was done to ensure that a few observations did not disproportionally affect the results. Further, all significant relationships were tested for non-linearity by introducing a quadratic term to a multiple regression analysis on the form $PES = C + \beta_1 age +$

$\beta_2 Var_1 + \beta_3(Var_1)^2 + \varepsilon$, where Var_1 is any brain variable (WM volume, DTI parameter), and nonlinearity was evidenced by $p<.05$ for β_3. To test whether an anterior–posterior gradient could be found for the relationships between PES and significant DTI measures, mean t-score was calculated for each slice in the anterior–posterior-direction, smoothed by locally estimated scatterplot smoothing and the results plotted across the range. This was done because frontal brain areas are assumed to be of special importance for PES (Aron et al., 2007; Danielmeier and Ullsperger, 2011). Finally, the best volumetric predictor and the best DTI predictor were entered into a multi-modal path analysis to model the contributions from the different imaging measures, as well as age, ICV and task performance. The path modeling was done implemented in AMOS 19, part of SPSS 19.

Since several of the covariates were expected to correlate, regression diagnostic analyses were run to avoid multi-collinearity. In no cases did the variance inflation factor approach a critical value of 10, or the tolerance a critical value of .10.

Results

PES, task performance and general ability level

Error rate was 5% in the congruent condition and 25% in the incongruent condition ($t[254] = 22.8$, $p<10^{-62}$). Mean RT for each correct congruent trial following an error trial was 404 ms, compared to 381 ms for the correct congruent trials that followed correct trials ($t = 8.3$ [254], $p<10^{-14}$). For incongruent trials, the difference between post-error and post-correct trials was not significant (475 vs. 473, t [254] = 1.0, n.s.). PES correlated positively with task performance for both congruent ($r = .26$, $p<10^{-4}$) and incongruent stimuli ($r = .20$, $p<.001$). PES did not correlate with general intellectual abilities (WASI verbal IQ $r = .08$, n.s.; performance IQ $r = .08$, n.s.; full scale IQ $r = .08$, n.s.). PES was negatively related to response variability, defined as the standard deviation of the mean RT divided by the mean for the correct congruent responses following an error (Partial $r = -.20$, $p<.001$, age and sex used as covariates.

WM morphometry

The relationships between WM volume and PES are shown in Fig. 2 and Table 1. Total WM volume correlated significantly with PES ($r = .15$, $p<.05$). Analyses at the level of lobes revealed that only the relationship for the frontal WM was statistically significant ($r = .22$, $p<.001$). The frontal relationship was replicated for both hemispheres (left $r = .24$, $p<.001$; right $r = .20$, $p = .001$). Thus, further analyses were done on the average of left and right ROIs. Within the frontal lobes, significant correlations with PES were found for the caudal ($r = .18$, $p<.01$) and rostral middle frontal ($r = .14$, $p<.05$) and

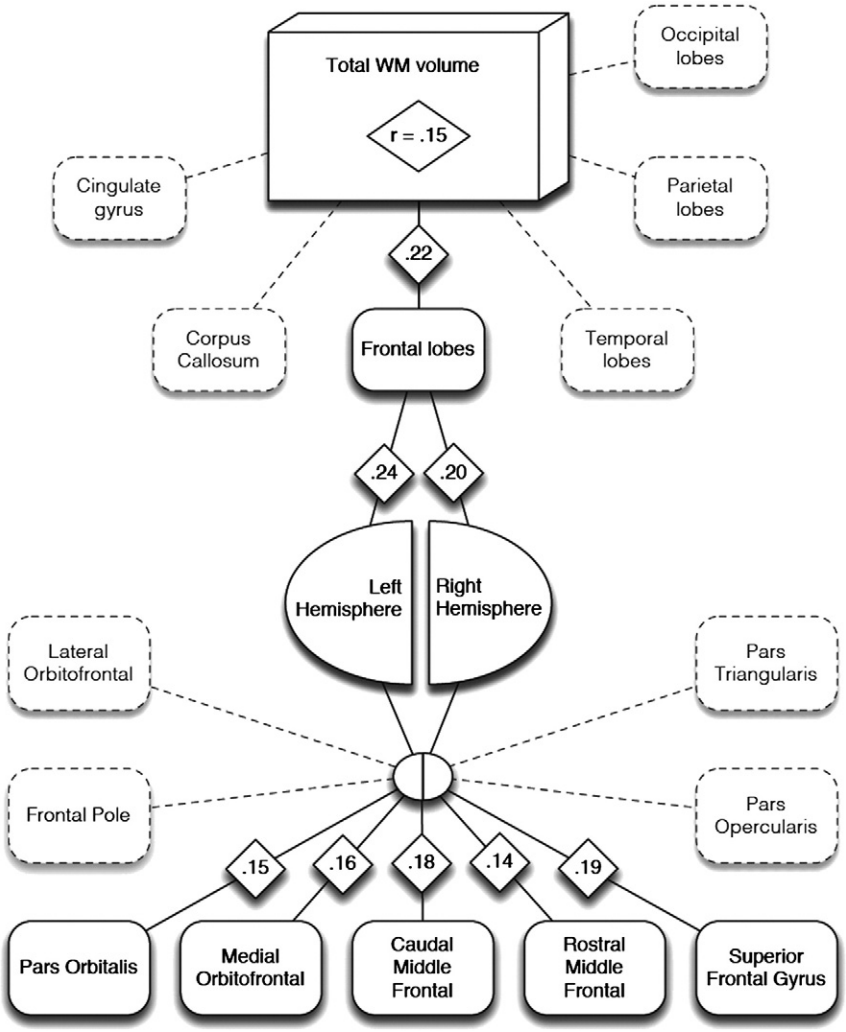

Fig. 2. Relationship between WM volume and post-error slowing. Partial correlations between post-error slowing and WM volume in different regions, corrected for age, intracranial volume and task performance.

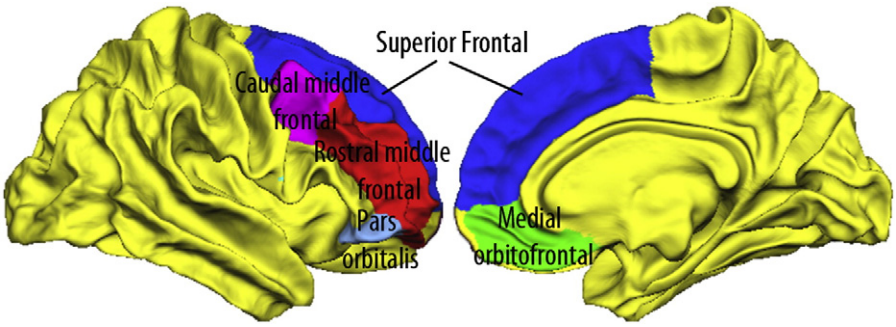

Fig. 3. Frontal regions where WM volume correlated significantly with post-error slowing, shown on the WM surface of a template brain.

superior frontal ($r=.19$, $p<.01$) gyri, medial orbitofrontal cortex ($r=.16$, $p<.05$) and pars orbitalis ($r=.15$, $p<.05$). Demarcation of the significant frontal ROIs are shown in Fig. 3.

The analyses were re-run with sex and task performance as additional covariates, which did not change the status from significant to non-significant or vice versa for any of the coefficients. Exclusion of statistical outliers (studentized deleted residuals >3 or <-3) did not render any of the significant relationships non-significant. For none of the variables was an interaction with age found (all $ps>.05$), and in no case did a quadratic term add significantly to the amount of explained variance. The analyses were re-run with non-normalized PES (not divided my mean RT) to ensure that the normalization procedure did not unduly affect the results. Pars orbitalis ($r=.12$, $p=.064$) and rostral middle frontal WM volumes ($r=.12$, $p=.06$) were then only marginally significant.

Thalamus volume

Thalamus volume correlated positively with PES ($r=.13$, $p<.05$) when age and ICV were partialled out. The correlations across hemispheres were almost identical (left $r=.123$, $p=.05$, right $r=.117$, $p=.062$). The analyses were re-run with task performance as an additional covariate, and the correlation was now only marginally significant ($r=.12$, $p=.056$). The analyses were also run with raw (non-normalized) PES scores. This did not affect the results much, but thalamus now correlated significantly with PES both when task performance in addition to age and ICV were included as covariates ($r=.13$, $p<.05$), and when only age and ICV were included as covariates ($r=.13$, $p<.05$). Exclusion of outliers rendered the correlation only marginally significant ($r=.10$, $p=.10$).

DTI

MD and AD were negatively related to PES as evidenced by whole-skeleton TBSS analyses ($p<.05$, corrected) when age was used as covariate (Fig. 4). For MD, significant relationships were found in 1086 voxels, mainly in the right superior longitudinal fasciculus, but also overlapping with the anterior thalamic radiation and an area that in the Johns Hopkins University (JHU) atlas (Hua et al., 2008; Wakana et al., 2004) is referred to as inferior fronto-occipital fasciculus (even though there is controversy regarding whether this tract actually exists, see e.g. (Schmahmann and Pandya, 2007)). For AD, 1717 voxels were significant, mainly in the body of the corpus callosum.

The partial correlations between mean MD and AD values across voxels significant at $p<.05$ and PES were computed, with age partialled out. MD and PES correlated $-.27$ and AD and PES $-.26$. Adding age, sex, task performance and total volume of WM T1 hypointensities did not affect the relationships much (MD $r=-.22$, AD $r=-.26$). An interaction with age did not approach significance. The relationships were further tested by fitting a quadratic function by adding AD^2 and MD^2 in turn to the models, which was not significant for either DTI measure. The analyses were re-run with outliers (studentized deleted residuals $<+/-3$) excluded. For both the MD and the AD analysis, this lead to the exclusion of four participants, and the partial correlation coefficients with PES were $-.21$ for AD and $-.25$ for AD (age partialled out), $p<.001$.

To test for anatomical specificity of the effect across the posterior–anterior axis, demeaned t-scores were plotted as a function of MNI y-coordinates, and the results fitted by locally weighted estimated scatter smoothing (LOESS) are shown in Fig. 5. As can be seen, for both MD and AD, the strongest effects were seen around MNI y-coordinate 0, shifted somewhat in the anterior direction.

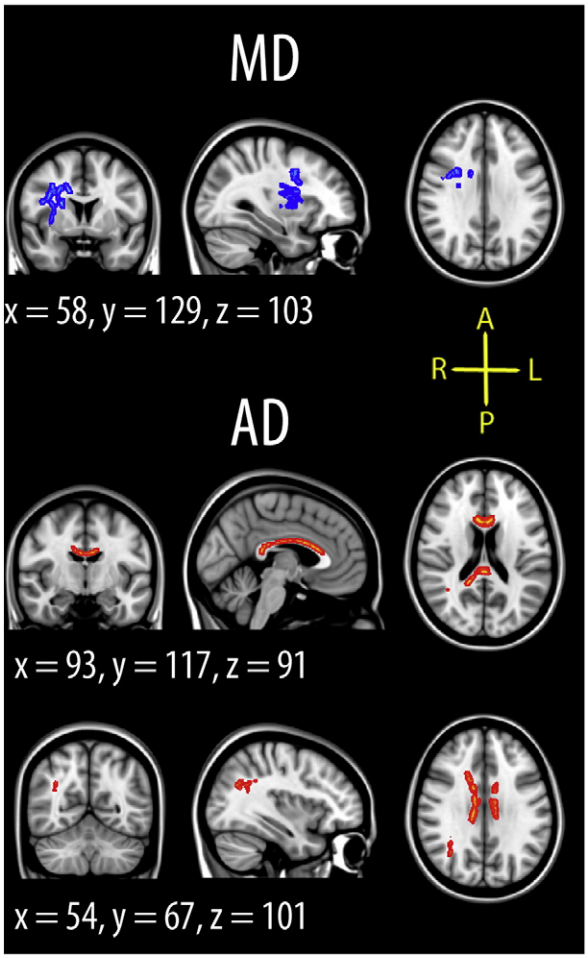

Fig. 4. Relationship between MD, AD and post-error slowing. Effects of post-error slowing on diffusion characteristics, corrected for age. The effects are corrected for multiple comparisons across space by threshold-free cluster enhancement (TFCE) at $p<.05$. The results are smoothed to ease visualization of effects. All relationships were negative.

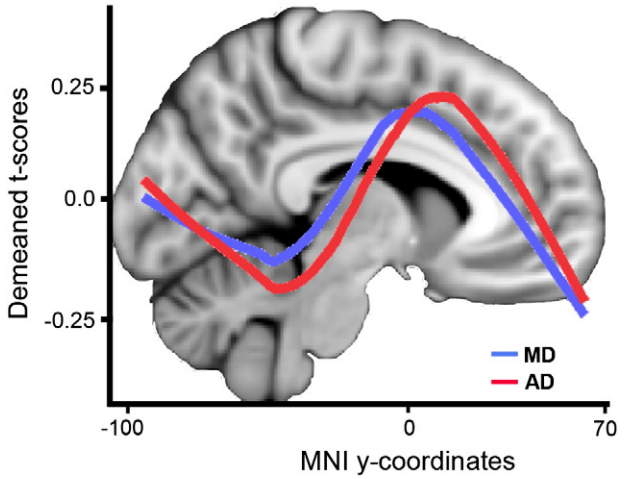

Fig. 5. Anterior–posterior gradients. The graphs represent demeaned t-values in the skeleton at each integer MNI y-coordinate for each DTI measure fitted by locally estimated scatterplot smoothing (LOESS). The number of skeleton voxels for each coordinate will vary, and thus the amount of white matter that is included. Coordinates with more included voxels, i.e. more white matter, may yield more accurate estimates. The graphs are projected on top of a template brain to illustrate the location along the y-axis. As can be seen, the strongest effects are located around coordinate 0, shifted somewhat in the anterior direction.

Multi-modal analysis

We wanted to model how the variance was distributed across the different variables of interest, and constructed a path model with PES, age, task performance, ICV, frontal WM volume and AD (see Fig. 6). Due to the problem of multi-collinearity caused by assumed high correlations between each of the volumetric measures on one hand and each of the DTI measures on the other, one WM volume structure and one DTI measure was selected. AD was chosen because this showed the strongest relationship to PES when age, sex, task performance and total volume of WM T1 hypointensities were covaried. The initial model included 12 paths. The relative chi square (CMIN/DF) of the model was 2.06, with a root mean square error of approximation (RMSEA) of .064, both of which indicate a good fit. However, several of the paths in the model were not significant. Thus, the paths with the highest p-value were recursively deleted, and the analysis re-run after each non-significant path was removed. This was repeated until a final model was reached. In this model, all paths were significant ($p<.05$). This final model showed an excellent fit, with a relative chi square of 1.06 and an RMSEA of .014. AD had a direct (−.24) effect on PES, as well as an indirect effect (−.04) through frontal WM volume, yielding a total effect of −.28. If the directionality of the AD ➔ frontal volume relationship was reversed (frontal volume ➔ AD), the model fit went down (CMIN/DF = 2.66/ RMSEA = .81), although still yielding a decent fit. In that model, however, the path from volume to AD was only marginally significant ($p=.084$). We also tested a model where AD was replaced by MD. In this model, all the paths were significant ($p<.05$), but the model fit was substantially reduced (CMIN/DF = 4.07/ RMSEA = .11).

Follow-up analyses of FA results

Only one previous study has investigated relationships between PES and DTI (Danielmeier et al., 2011). In that study, PES from 20 young participants was correlated with FA (no other DTI measures were reported), using TBSS, and effects were identified in WM beneath left anterior midcingulate cortex (AMC) and right pre-supplementary motor area (pre-SMA). However, while a statistical threshold of $p<.05$, fully corrected for multiple comparisons across space by permutation testing, was used in the present paper, the previous study used an uncorrected threshold of $p<.001$ with a minimum cluster size of 40 contiguous voxels. Since the latter approach is less conservative, we thresholded our statistical maps from the FA analyses at $p<.001$ to allow more direct comparison of results across studies. This revealed a cluster of 45 contiguous voxels located in the WM underneath left precentral gyrus and partly underneath middle frontal gyrus (peak effect at $x=-36$, $y=-1$, $z=30$). In addition, we found a cluster located beneath the precentral and opercular cortices in the right hemisphere (peak effect at $x=38$, $y=-5$, $z=26$). The latter cluster contained only 26 contiguous voxels significant at $p<.001$ (uncorrected), but was included here for purpose of comparison with Danielmeier et al. These clusters are shown in Fig. 7.

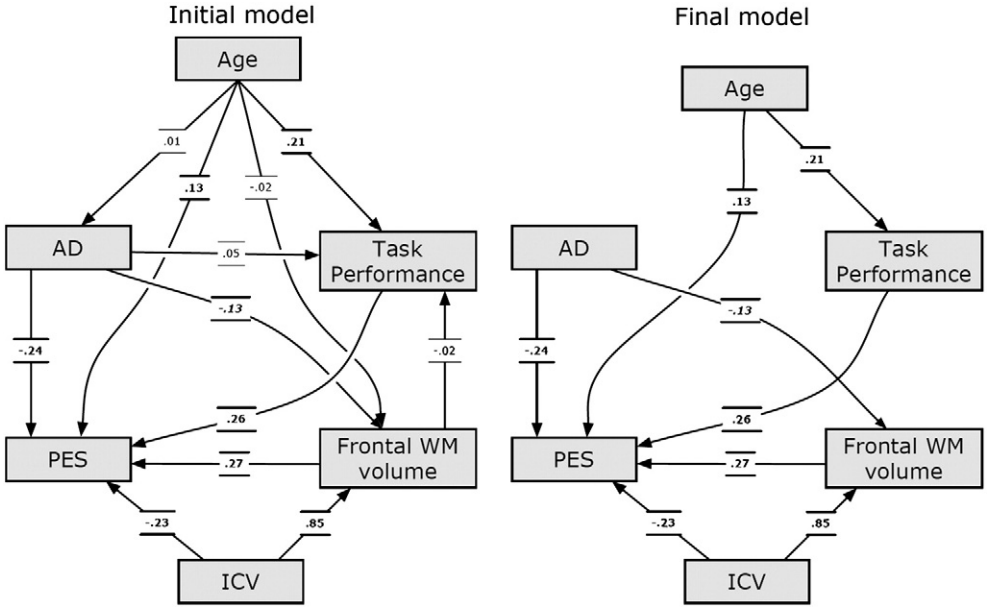

Fig. 6. Multi-modal path analysis. Path analysis was used to test how the relationship between the different predictor variables and PES. In the initial model, several of the paths were not significant. The paths with the highest p-value above .05 were deleted recursively one-by-one, and the analyses re-run after each path was removed. In the final model, all paths are significant. Standardized regression weights for the significant paths are shown next to each path arrow. Bold characters indicate $p<.01$.

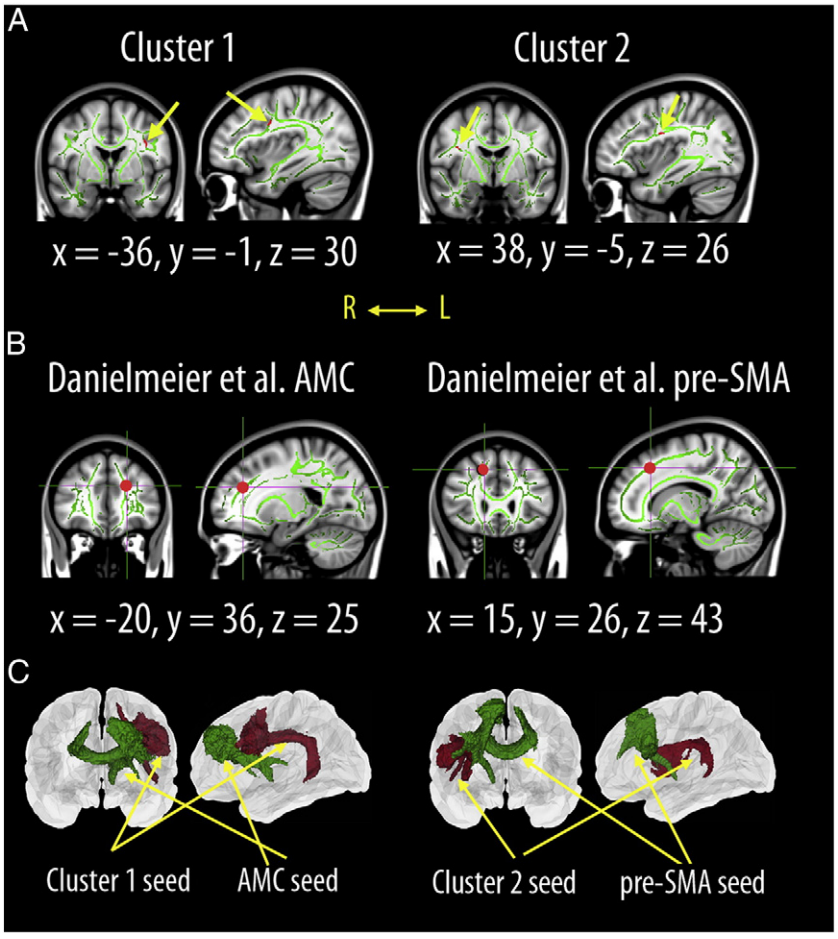

Fig. 7. Tractography. Panel A: To test whether we could replicate the relationship between FA and PES found by Danielmeier et al. (2011), the TBSS analyses were re-run for FA with a different statistical threshold employed ($p<.001$, uncorrected, minimum cluster size 40 contiguous voxels). Cluster 1 satisfied this criterion, while cluster 2 only consisted of 26 contiguous voxels but was still included for comparison purposes. The clusters are indicated by the yellow arrows. Panel B: The peak voxel of effect in each of the two clusters identified by Danielmeier et al. (2011) illustrated by the red dots. Note that the dots represent a circular extension (diameter of 20 pixels) of the peak voxel of the original effects, and not the actual cluster reported by Danielmeier et al. Panel C: Tractography was performed for a subsample of 60 randomly selected participants. The red tracts are mean projections across participants using each of the two clusters identified in the current study as seeds. The green voxels are thresholded and averaged distributions from the clusters reported in Danielmeier et al. Note that the latter seeds were generated by dilating the voxels of maximum effects from Danielmeier et al. in two steps, yielding 125 contiguous voxels as seed points in each case. As can be seen, the tracts from the different seed points are clearly distinguishable.

To test whether these clusters were parts of the same structural network identified by Danielmeier et al., we performed probabilistic tractography using the significant voxels from our own analyses as seed points, and compared the results with the results of running the tractography by use of the peak voxels reported in Danielmeier et al. (dilated in all three dimensions in two steps using fslmaths, yielding a total of 125 voxels) (see Fig. 7). Tractography from our approximation of the effects obtained by Danielmeier et al. yielded tracts crossing the corpus callosum into the opposite hemisphere, similar to what was obtained in the original study. However, tractography from the clusters identified in the present study yielded tracts following the anterior–posterior axis, likely connecting the frontal lobes and more posterior areas of the brain. These tracts overlapped with the superior longitudinal fasciculus. Although the clusters identified across studies were situated not too far from each other, the probabilistic tractography did not lend strong support to the hypothesis that they feed into the same major WM pathways.

Discussion

This study is the first extensive attempt to map the structural brain correlates of PES, and the results indicate that WM properties are associated with stronger PES. This association was seen both at a macro- and a microstructural level. In addition, the multi-modal analysis showed that WM volume and WM tissue DTI characteristics were independent contributors to the variance in PES. Thus, the ability to adjust behavior in response to commission of an error is related to different WM properties. The implications of these results are discussed below.

In a speeded continuous performance tasks, occasional errors are hard to avoid. PES is an important mean to adjust behavior in order to minimize the likelihood of a second error (Rabbitt, 1966). PES likely reflects an increased degree of controlled responding, and provides more time for task-focused visual encoding (Danielmeier et al., 2011). In a recent review, Danielmeier and Ullsperger argue that PES may be related to cognitive control mechanisms, inhibition or reflecting an orienting response, and that these explanations not necessarily are mutually exclusive (Danielmeier and Ullsperger, 2011). The present results suggest that the degree to which a participant is able to make such post-error adjustments of behavior partly depends on WM characteristics. These relationships were linear, indicating no difference between maximal and optimal PES. Further, no age-interactions were found, which means that the relationships between PES and WM characteristics did not change across life, as one could expect if these were caused by accumulation of WM lesion load. First, larger WM volumes in several frontal regions were positively correlated with PES. The crucial role of the frontal lobes in cognitive control is well established (Miller and D'Esposito, 2005), and the medial frontal cortex is likely of particular importance (Ridderinkhof et

al., 2004). Danielmeier et al. (2011) demonstrated that medial frontal cortex activity modulates post-error adaptations in other parts of the brain, i.e. task-related visual and motor areas. In the present study, PES correlated with WM volume in the frontal lobe only, and subsequent analyses confined the relationships to caudal and rostral middle and superior frontal, medial orbitofrontal gyri and pars orbitalis. This fits well with the known importance of these areas for various tasks related to cognitive control. Cingulate WM volume was not related to PES, even though this region is involved in a variety of control tasks (Bush et al., 2000), particularly when the experienced probability of committing an error is high (Brown and Braver, 2005). The explanation may be that WM effects are less likely to be anatomically confined compared to gray matter effects (Westlye et al., 2011), as the main function of the WM tracts is transfer of information between distant cortical and subcortical areas. Thus, input from e.g. anterior cingulate to the orbitofrontal cortex will depend on WM connections in areas where significant effects were identified in the present study, even though PES was not related to WM volume directly underneath the cingulate cortices. For instance, we have previously shown that the cingulum bundle constitutes a major part of the WM underneath the superior frontal gyrus, and that FA in the cingulum bundle correlates with FA in WM here as well as in WM underneath the medial orbitofrontal gyrus (Fjell et al., 2008), for both of which a relationship between WM volume and PES was seen.

Relationships between WM microstructure and PES were found for MD and AD. Less diffusion, in terms of lower AD and MD, was related to higher PES. DTI is based on the random displacement of water molecules in the tissue, and the neurobiological underpinnings affecting the level of diffusion includes myelination, axonal integrity and axonal packing (Concha et al., 2006, 2010; Song et al., 2002, 2003). More restricted diffusion is generally regarded as an index of higher WM integrity, and MD and AD increases in aging (Madden et al., 2012; Westlye et al., 2010) and Alzheimer's Disease (Agosta et al., 2011) have been found. Thus, the DTI results were in general agreement with the WM volume analyses, indicating a positive relationship between PES and WM integrity.

The relationships between PES and the DTI measures were confined to specific WM tracts. For AD, relationships with PES were seen throughout the corpus callosum, especially in the body, hardly intersecting other major tracts. MD-PES relationships were found in the right hemisphere only, mainly in the superior longitudinal fasciculus (SLF). Further, some effects were also seen in the anterior thalamic radiation (ATR) and in the area referred to in the JHU atlas as the inferior fronto-occipital fasciculus (IFOF). SLF connects the parietal lobe association cortices with the frontal lobe, and travels through parts of the WM of the superior frontal gyrus, terminating in dorsolateral and -medial frontal cortices (Schmahmann and Pandya, 2006), partly corresponding to the volumetric effects seen. ATR consists of fibers connecting the anterior and medial thalamic nuclei and the cerebral cortex of the frontal lobe, conveying fibers from all regions of the prefrontal cortex, as well as from the supplementary motor area (Schmahmann and Pandya, 2006). Interestingly, a relationship between thalamic volume and PES was also observed in the present study (or a trend level, depending of the exact nature of the analysis). IFOF is anatomically located so that it is likely that fibers in this area connects the occipital and frontal lobes via the temporal lobe (Kier et al., 2004), originating from, among other areas, the caudal cingulate gyrus, conveying visual information predominantly to the dorsal premotor and dorsal prefrontal cortices, engaged in higher-order aspects of motor behavior and attention (Schmahmann and Pandya, 2006). Thus, all effects of PES on AD intersected tracts involved in transfer of information between the frontal cortex and other parts of the brain, in coherence with an account of PES as related to or indexing cognitive control, alerting or inhibition (Danielmeier and Ullsperger, 2011), functions known to depend heavily of frontal circuits (Miller and D'Esposito, 2005). Fig. 5, showing the smoothed demeaned t-values as a function of voxel coordinates along the posterior–anterior axis, may also yield some support to the notion of a more frontal than posterior pattern of effects, although the effect sizes drop after the middle section of the corpus callosum.

Although we have lacked fundamental knowledge about how structural brain characteristics affects PES in healthy participants, one recent study tested the relationship between DTI and PES. In a sample of 20 young adults, PES correlated with FA in WM beneath posterior mid-frontal cortex regions that were connected to the motor inhibition system (Danielmeier et al., 2011), providing evidence for a relationship between PES and WM integrity. In the present study, relationships were found between PES and MD and AD. Danielmeier et al. did not report results from other DTI measures, so the results are not directly comparable. Still, both studies yield some evidence for a positive relationship between higher WM integrity and greater PES, although with notable differences. With use of a liberal statistical threshold to allow more direct comparisons with the previous study, we were able to identify two clusters where FA correlated positively with PES, in accordance with what one would have expected based on the results of Danielmeier et al. Both of these clusters were in proximity to the precentral gyrus, which was shown to be related to functional MRI activity change associated with PES (Danielmeier et al., 2011). However, tractography indicated that these clusters were located in different major pathways compared to the two clusters found by Danielmeier et al. Thus, the results for FA seem replicable across two independent studies regarding the extension and direction of effects, but not necessarily regarding the anatomical location of the effects. Still, we believe that the present results and the results from Danielmeier et al. strengthen the case that WM microstructure is related to individual differences in PES. This also fits nicely with the results of previous studies that have found positive correlations between FA in the posterior cingulate and both the amplitude of the ERN (Westlye et al., 2009) and the speed of self-corrections after error responses (Agam et al., 2011).

Finally, the multi-modal analysis demonstrated that WM macro- and microstructure independently contributed to explain PES. Both measures are regarded as indexing WM integrity (Salat et al., 2005), but the relationships between the two are modest in healthy populations (Fjell et al., 2008; Tamnes et al., 2010). The present results showed that WM volume and DTI parameters were about equally strongly related to PES. This underscores that WM macro- and microstructure both represent biologically interesting properties of WM, related to cognitive function, and that both levels of analysis can be included to get a more comprehensive account of the neurocognitive significance of individual differences in WM structure. This was clearly seen from the path analysis, where a model where both classes of measures were included together with age, task performance and ICV yielded an excellent fit.

Further research should also test how response variability fits into this picture, as response variability were negatively related to PES, and relationships between response variability and WM microstructure have recently been reported (Fjell et al., 2011; Tamnes et al., 2012). Also, the present study yielded some evidence for thalamic volume as a predictor of PES, but the relationship was weak, and was only marginally significant in the outlier analyses. Thalamus is anatomically well connected and functionally closely interacting with anterior cingulate and previous research has given evidence that thalamic injury affects PES (Peterburs et al., 2011; Seifert et al., 2011). Thus, future efforts should focus more on the possible role of structural properties of the thalamus also in healthy populations.

In conclusion, individual differences in the degree to which a person is able to adjust his or her behavior to optimize performance in speeded cognitive tasks are related to properties of the WM, both at a macro- and a microstructural level. This provides insights into the brain structural correlates of cognitive control. Future research should also try to elucidate whether changes in the WM foundation for PES

can account for diminished abilities of behavioral adjustment in various clinical groups with reduced levels of cognitive control, e.g. fronto-temporal dementia (Collette et al., 2010) and attention-deficit hyperactivity disorder (Spinelli et al., 2011).

Acknowledgments

This work was supported by the Norwegian Research Council (grant number 204966 to L.T.W; 77404 and 186092 to K.B.W; 175066 and 189507 to A.M.F.) and the University of Oslo (to K.B.W. and A.M.F).

References

Agam, Y., Hamalainen, M.S., Lee, A.K., Dyckman, K.A., Friedman, J.S., Isom, M., Makris, N., Manoach, D.S., 2011. Multimodal neuroimaging dissociates hemodynamic and electrophysiological correlates of error processing. Proc. Natl. Acad. Sci. U. S. A. 108, 17556–17561.

Agosta, F., Pievani, M., Sala, S., Geroldi, C., Galluzzi, S., Frisoni, G.B., Filippi, M., 2011. White matter damage in Alzheimer disease and its relationship to gray matter atrophy. Radiology 258, 853–863.

Andersson, J.L.R., Jenkinson, M., Smith, S., 2007a. Non-linear optimisation. FMRIB technical report TR07JA1. from www.fmriboxacuk/analysis/techrep.

Andersson, J.L.R., Jenkinson, M., Smith, S., Andersson, J.L.R., Jenkinson, M., Smith, S., 2007b. Non-linear registration, aka Spatial normalisation. FMRIB technical report TR07JA2. from www.fmriboxacuk/analysis/techrep.

Aron, A.R., Behrens, T.E., Smith, S., Frank, M.J., Poldrack, R.A., 2007. Triangulating a cognitive control network using diffusion-weighted magnetic resonance imaging. MRI. and functional MRI. J. Neurosci. 27, 3743–3752.

Beck, A.T., Steer, R., 1987. Beck Depression Inventory Scoring Manual. The Psychological Corporation, New York.

Behrens, T.E., Woolrich, M.W., Jenkinson, M., Johansen-Berg, H., Nunes, R.G., Clare, S., Matthews, P.M., Brady, J.M., Smith, S.M., 2003. Characterization and propagation of uncertainty in diffusion-weighted MR imaging. Magn. Reson. Med. 50, 1077–1088.

Behrens, T.E., Berg, H.J., Jbabdi, S., Rushworth, M.F., Woolrich, M.W., 2007. Probabilistic diffusion tractography with multiple fibre orientations: what can we gain? Neuroimage 34, 144–155.

Bernstein, P.S., Scheffers, M.K., Coles, M.G., 1995. "Where did I go wrong?" A psychophysiological analysis of error detection. J. Exp. Psychol. Hum. Percept. Perform. 21, 1312–1322.

Bravo, G., Hebert, R., 1997. Age- and education-specific reference values for the Mini-Mental and modified Mini-Mental State Examinations derived from a non-demented elderly population. Int. J. Geriatr. Psychiatry 12, 1008–1018.

Brown, J.W., Braver, T.S., 2005. Learned predictions of error likelihood in the anterior cingulate cortex. Science 307, 1118–1121.

Buckner, R.L., Head, D., Parker, J., Fotenos, A.F., Marcus, D., Morris, J.C., Snyder, A.Z., 2004. A unified approach for morphometric and functional data analysis in young, old, and demented adults using automated atlas-based head size normalization: reliability and validation against manual measurement of total intracranial volume. Neuroimage 23, 724–738.

Bush, G., Luu, P., Posner, M.I., 2000. Cognitive and emotional influences in anterior cingulate cortex. Trends Cogn. Sci. 4, 215–222.

Collette, F., Van der Linden, M., Salmon, E., 2010. Dissociation between controlled and automatic processes in the behavioral variant of fronto-temporal dementia. J. Alzheimers Dis. 22, 897–907.

Concha, L., Gross, D.W., Wheatley, B.M., Beaulieu, C., 2006. Diffusion tensor imaging of time-dependent axonal and myelin degradation after corpus callosotomy in epilepsy patients. Neuroimage 32, 1090–1099.

Concha, L., Livy, D.J., Beaulieu, C., Wheatley, B.M., Gross, D.W., 2010. In vivo diffusion tensor imaging and histopathology of the fimbria-fornix in temporal lobe epilepsy. J. Neurosci. 30, 996–1002.

Dale, A.M., Fischl, B., Sereno, M.I., 1999. Cortical surface-based analysis. I. Segmentation and surface reconstruction. Neuroimage 9, 179–194.

Danielmeier, C., Ullsperger, M., 2011. Post-error adjustments. Front. Psychol. 2, 233.

Danielmeier, C., Eichele, T., Forstmann, B.U., Tittgemeyer, M., Ullsperger, M., 2011. Posterior medial frontal cortex activity predicts post-error adaptations in task-related visual and motor areas. J. Neurosci. 31, 1780–1789.

Debener, S., Ullsperger, M., Siegel, M., Fiehler, K., von Cramon, D.Y., Engel, A.K., 2005. Trial-by-trial coupling of concurrent electroencephalogram and functional magnetic resonance imaging identifies the dynamics of performance monitoring. J. Neurosci. 25, 11730–11737.

Desikan, R.S., Segonne, F., Fischl, B., Quinn, B.T., Dickerson, B.C., Blacker, D., Buckner, R.L., Dale, A.M., Maguire, R.P., Hyman, B.T., Albert, M.S., Killiany, R.J., 2006. An automated labeling system for subdividing the human cerebral cortex on MRI scans into gyral based regions of interest. Neuroimage 31, 968–980.

Eriksen, B.A., Eriksen, C.W., 1974. Effects of noise letters upon the identification of a target letter in a nonsearch task. Percept. Psychophys. 16, 143–149.

Falkenstein, M., Hohnsbein, J., Hoormann, J., Blanke, L., 1991. Effects of cross-modal divided attention on late ERP components: II. Error processing in choice reaction tasks. Electroencephalogr. Clin. Neurophysiol. 78, 447–455.

Fischl, B., Dale, A.M., 2000. Measuring the thickness of the human cerebral cortex from magnetic resonance images. Proc. Natl. Acad. Sci. U. S. A. 97, 11050–11055.

Fischl, B., Sereno, M.I., Dale, A.M., 1999a. Cortical surface-based analysis. II: inflation, flattening, and a surface-based coordinate system. Neuroimage 9, 195–207.

Fischl, B., Sereno, M.I., Tootell, R.B., Dale, A.M., 1999b. High-resolution intersubject averaging and a coordinate system for the cortical surface. Hum. Brain Mapp. 8, 272–284.

Fischl, B., Liu, A., Dale, A.M., 2001. Automated manifold surgery: constructing geometrically accurate and topologically correct models of the human cerebral cortex. IEEE Trans. Med. Imaging 20, 70–80.

Fischl, B., Salat, D.H., Busa, E., Albert, M., Dieterich, M., Haselgrove, C., van der Kouwe, A., Killiany, R., Kennedy, D., Klaveness, S., Montillo, A., Makris, N., Rosen, B., Dale, A.M., 2002. Whole brain segmentation: automated labeling of neuroanatomical structures in the human brain. Neuron 33, 341–355.

Fischl, B., Salat, D.H., van der Kouwe, A.J., Makris, N., Segonne, F., Quinn, B.T., Dale, A.M., 2004a. Sequence-independent segmentation of magnetic resonance images. Neuroimage 23 (Suppl. 1), S69–S84.

Fischl, B., van der Kouwe, A., Destrieux, C., Halgren, E., Segonne, F., Salat, D.H., Busa, E., Seidman, L.J., Goldstein, J., Kennedy, D., Caviness, V., Makris, N., Rosen, B., Dale, A.M., 2004b. Automatically parcellating the human cerebral cortex. Cereb. Cortex 14, 11–22.

Fjell, A.M., Westlye, L.T., Greve, D.N., Fischl, B., Benner, T., van der Kouwe, A.J., Salat, D., Bjornerud, A., Due-Tonnessen, P., Walhovd, K.B., 2008. The relationship between diffusion tensor imaging and volumetry as measures of white matter properties. Neuroimage 42, 1654–1668.

Fjell, A.M., Westlye, L.T., Amlien, I., Walhovd, K.B., 2011. Reduced white matter integrity is related to cognitive instability. J. Neurosci. 31, 18060–18072.

Folstein, M.F., Folstein, S.E., McHugh, P.R., 1975. "Mini-mental state". A practical method for grading the cognitive state of patients for the clinician. J. Psychiatr. Res. 12, 189–198.

Gehring, W.J., Knight, R.T., 2000. Prefrontal–cingulate interactions in action monitoring. Nat. Neurosci. 3, 516–520.

Gehring, W.J., Goss, B., Coles, M.G.H., Meyer, D.E., Donchin, E., 1993. A neural system for error detection and compensation. Psychol. Sci. 4, 385–390.

Hogan, A.M., Vargha-Khadem, F., Saunders, D.E., Kirkham, F.J., Baldeweg, T., 2006. Impact of frontal white matter lesions on performance monitoring: ERP evidence for cortical disconnection. Brain 129, 2177–2188.

Hua, K., Zhang, J., Wakana, S., Jiang, H., Li, X., Reich, D.S., Calabresi, P.A., Pekar, J.J., van Zijl, P.C., Mori, S., 2008. Tract probability maps in stereotaxic spaces: analyses of white matter anatomy and tract-specific quantification. Neuroimage 39, 336–347.

Jenkinson, M., Smith, S., 2001. A global optimisation method for robust affine registration of brain images. Med. Image Anal. 5, 143–156.

Jenkinson, M., Bannister, P., Brady, M., Smith, S., 2002. Improved optimization for the robust and accurate linear registration and motion correction of brain images. Neuroimage 17, 825–841.

Kier, E.L., Staib, L.H., Davis, L.M., Bronen, R.A., 2004. MR imaging of the temporal stem: anatomic dissection tractography of the uncinate fasciculus, inferior occipitofrontal fasciculus, and Meyer's loop of the optic radiation. AJNR Am. J. Neuroradiol. 25, 677–691.

Madden, D.J., Bennett, I.J., Burzynska, A., Potter, G.G., Chen, N.K., Song, A.W., 2012. Diffusion tensor imaging of cerebral white matter integrity in cognitive aging. Biochim. Biophys. Acta 1822, 386–400.

Miller, B.T., D'Esposito, M., 2005. Searching for "the top" in top-down control. Neuron 48, 535–538.

Nichols, T.E., Holmes, A.P., 2002. Nonparametric permutation tests for functional neuroimaging: a primer with examples. Hum. Brain Mapp. 15, 1–25.

Peterburs, J., Pergola, G., Koch, B., Schwarz, M., Hoffmann, K.P., Daum, I., Bellebaum, C., 2011. Altered error processing following vascular thalamic damage: evidence from an antisaccade task. PLoS One 6, e21517.

Rabbitt, P.M., 1966. Errors and error correction in choice-response tasks. J. Exp. Psychol. 71, 264–272.

Reese, T.G., Heid, O., Weisskoff, R.M., Wedeen, V.J., 2003. Reduction of eddy-current-induced distortion in diffusion MRI using a twice-refocused spin echo. Magn. Reson. Med. 49, 177–182.

Ridderinkhof, K.R., Ullsperger, M., Crone, E.A., Nieuwenhuis, S., 2004. The role of the medial frontal cortex in cognitive control. Science 306, 443–447.

Rovaris, M., Comi, G., Rocca, M.A., Cercignani, M., Colombo, B., Santuccio, G., Filippi, M., 1999. Relevance of hypointense lesions on fast fluid-attenuated inversion recovery MR images as a marker of disease severity in cases of multiple sclerosis. AJNR Am. J. Neuroradiol. 20, 813–820.

Rueckert, D., Sonoda, L.I., Hayes, C., Hill, D.L., Leach, M.O., Hawkes, D.J., 1999. Nonrigid registration using free-form deformations: application to breast MR images. IEEE Trans. Med. Imaging 18, 712–721.

Salat, D.H., Tuch, D.S., Hevelone, N.D., Fischl, B., Corkin, S., Rosas, H.D., Dale, A.M., 2005. Age-related changes in prefrontal white matter measured by diffusion tensor imaging. Ann. N. Y. Acad. Sci. 1064, 37–49.

Salat, D.H., Greve, D.N., Pacheco, J.L., Quinn, B.T., Helmer, K.G., Buckner, R.L., Fischl, B., 2009. Regional white matter volume differences in nondemented aging and Alzheimer's disease. Neuroimage 44, 1247–1258.

Schmahmann, J.D., Pandya, D.N., 2006. Fiber Pathways of the Brain. Oxford University Press, Oxford.

Schmahmann, J.D., Pandya, D.N., 2007. The complex history of the fronto-occipital fasciculus. J. Hist. Neurosci. 16, 362–377.

Segonne, F., Dale, A.M., Busa, E., Glessner, M., Salat, D., Hahn, H.K., Fischl, B., 2004. A hybrid approach to the skull stripping problem in MRI. Neuroimage 22, 1060–1075.

Seifert, S., von Cramon, D.Y., Imperati, D., Tittgemeyer, M., Ullsperger, M., 2011. Thalamocingulate interactions in performance monitoring. J. Neurosci. 31, 3375–3383.

Smith, S.M., 2002. Fast robust automated brain extraction. Hum. Brain Mapp. 17, 143–155.
Smith, S.M., Nichols, T.E., 2009. Threshold-free cluster enhancement: addressing problems of smoothing, threshold dependence and localisation in cluster inference. Neuroimage 44, 83–98.
Smith, S.M., Jenkinson, M., Woolrich, M.W., Beckmann, C.F., Behrens, T.E., Johansen-Berg, H., Bannister, P.R., De Luca, M., Drobnjak, I., Flitney, D.E., Niazy, R.K., Saunders, J., Vickers, J., Zhang, Y., De Stefano, N., Brady, J.M., Matthews, P.M., 2004. Advances in functional and structural MR image analysis and implementation as FSL. Neuroimage 23 (Suppl. 1), S208–S219.
Smith, S.M., Jenkinson, M., Johansen-Berg, H., Rueckert, D., Nichols, T.E., Mackay, C.E., Watkins, K.E., Ciccarelli, O., Cader, M.Z., Matthews, P.M., Behrens, T.E., 2006. Tract-based spatial statistics: voxelwise analysis of multi-subject diffusion data. Neuroimage 31, 1487–1505.
Smith, S.M., Johansen-Berg, H., Jenkinson, M., Rueckert, D., Nichols, T.E., Miller, K.L., Robson, M.D., Jones, D.K., Klein, J.C., Bartsch, A.J., Behrens, T.E., 2007. Acquisition and voxelwise analysis of multi-subject diffusion data with tract-based spatial statistics. Nat. Protoc. 2, 499–503.
Song, S.K., Sun, S.W., Ramsbottom, M.J., Chang, C., Russell, J., Cross, A.H., 2002. Dysmyelination revealed through MRI as increased radial. but unchanged axial. diffusion of water. Neuroimage 17, 1429–1436.
Song, S.K., Sun, S.W., Ju, W.K., Lin, S.J., Cross, A.H., Neufeld, A.H., 2003. Diffusion tensor imaging detects and differentiates axon and myelin degeneration in mouse optic nerve after retinal ischemia. Neuroimage 20, 1714–1722.
Spinelli, S., Vasa, R.A., Joel, S., Nelson, T.E., Pekar, J.J., Mostofsky, S.H., 2011. Variability in post-error behavioral adjustment is associated with functional abnormalities in the temporal cortex in children with ADHD. J. Child Psychol. Psychiatry 52, 808–816.
Stemmer, B., Segalowitz, S.J., Witzke, W., Schonle, P.W., 2004. Error detection in patients with lesions to the medial prefrontal cortex: an ERP study. Neuropsychologia 42, 118–130.
Tamnes, C.K., Ostby, Y., Fjell, A.M., Westlye, L.T., Due-Tonnessen, P., Walhovd, K.B., 2010. Brain maturation in adolescence and young adulthood: regional age-related changes in cortical thickness and white matter volume and microstructure. Cereb. Cortex 20, 534–548.
Tamnes, C.K., Fjell, A.M., Westlye, L.T., Ostby, Y., Walhovd, K.B., 2012. Becoming consistent: developmental reductions in intraindividual variability in reaction time are related to white matter integrity. J. Neurosci. 32, 972–982.
Ullsperger, M., von Cramon, D.Y., 2006. The role of intact frontostriatal circuits in error processing. J. Cogn. Neurosci. 18, 651–664.
Verguts, T., Notebaert, W., Kunde, W., Wuhr, P., 2011. Post-conflict slowing: cognitive adaptation after conflict processing. Psychon. Bull. Rev. 18, 76–82.
Wakana, S., Jiang, H., Nagae-Poetscher, L.M., van Zijl, P.C., Mori, S., 2004. Fiber tract-based atlas of human white matter anatomy. Radiology 230, 77–87.
Wechsler, D., 1999. Wechsler Abbreviated Scale of Intelligence. The Psychological Corporation, San Antonio, TX.
Westlye, L.T., Walhovd, K.B., Bjørnerud, A., Due-Tønnessen, P., Fjell, A.M., 2009. Error-related negativity is mediated by fractional anisotropy in the posterior cingulate gyrus—a study combining diffusion tensor imaging and electrophysiology in healthy adults. Cereb. Cortex 19, 293–304.
Westlye, L.T., Walhovd, K.B., Dale, A.M., Bjornerud, A., Due-Tonnessen, P., Engvig, A., Grydeland, H., Tamnes, C.K., Ostby, Y., Fjell, A.M., 2010. Life-span changes of the human brain white matter: diffusion tensor imaging. DTI. and volumetry. Cereb. Cortex 20, 2055–2068.
Westlye, L.T., Grydeland, H., Walhovd, K.B., Fjell, A.M., 2011. Associations between regional cortical thickness and attentional networks as measured by the attention network test. Cereb. Cortex 21, 345–356.
Woolrich, M.W., Jbabdi, S., Patenaude, B., Chappell, M., Makni, S., Behrens, T., Beckmann, C., Jenkinson, M., Smith, S.M., 2009. Bayesian analysis of neuroimaging data in FSL. Neuroimage 45, S173–S186.